Optimization of Permanent Magnet Synchronous Motors Using Conformal Mappings

Behrooz Rezaeealam* and Farhad Rezaee-Alam

Department of Electrical Engineering, Lorestan University, Khorramabad, Lorestan, 68137-17133, Iran
*rezaeealam@gmail.com

Abstract ─ An optimal permanent magnet synchronous motor (PMSM) should be a low cogging torque and a sinusoidal back-EMF. In this paper, different magnetizations and shaping models of permanent magnets (PMs) are investigated for achieving an optimal performance. The technique of slot opening shift is simultaneously implemented on the stator slots for more reducing of the cogging torque. To this end, the conformal mapping (CM) method as an accurate and fast technique is used to calculate the motor performance under each condition. In final, the optimal results obtained through the CM method are verified by comparing with the corresponding results obtained from the finite element method (FEM).

Index Terms ─ Cogging torque, conformal mapping (CM), magnetization, permanent magnet (PM), sinusoidal shaping (sin-shaping), slot opening shift.

I. INTRODUCTION

Due to high power density and high efficiency, the permanent magnet synchronous motors (PMSMs) are increasingly used in different industrial applications from automotive to aerospace. For this reason, the performance of PMSMs should be optimal as far as possible. To optimize the performance of PMSMs, it is necessary to shape the air gap magnetic field distribution in sinusoidal and to reduce the cogging torque.

So far, different techniques have been introduced for shaping the air gap magnetic field distribution. These techniques are divided into three groups: (a) the techniques based on the magnetization of PMs [1], (b) the techniques based on the shaping of PMs [2-4], and (c) the hybrid techniques based on the magnetization and the magnet shaping, simultaneously [5].

There are three types of PM magnetization, radial, parallel, and Halbach magnetization. The radial magnetization is usually suitable for PM BLDC machines, whereas the parallel and Halbach magnetizations are usually used in PM BLAC machines. The shaping techniques, including the sinusoidal shaping (sin-shaping) [5], the inverse cosine air gap shaping [5], and the loaf shape [6] are used to sinusoidally shape the air gap flux density and to save the magnet material, simultaneously. These techniques are nearly efficient for cogging torque reduction too.

There are also various techniques for cogging torque reduction more efficiently, such as PM or slot skewing [7-8], magnet segmentation [9], fractional slot winding [10], asymmetrical distribution of magnet poles [11] or stator tooth width [12] and so on. However, the motor performance drops by using the majority of these methods in addition to the cogging torque reduction. For this reason, the slot opening shift method is also used in this paper to more reduce the cogging torque, without reduction in the motor performance. So far, different modeling techniques have been used to calculate the cogging torque and the magnetic field distribution due to shaping and magnetization of permanent magnets, such as FEM and subdomain model [5]. The subdomain model acts based on the solving of governing equations in all subdomains, including air gap, PMs, slots, and slot openings [13-14].

In this paper, the CM method is used to calculate the air gap magnetic field, back-EMF, and cogging torque. The CM method acts based on the complex analysis. Carter used the CMs to calculate the suitable coefficients (Carter's coefficients) for considering the slotting effect. Zhu introduced a relative permeance function to consider the slotting effect in air gap magnetic field distribution [15]. However, this relative permeance function cannot consider the tangential component of air gap flux density. To remove this defect, zarko introduced the complex permeance model which can consider the radial and the tangential components of air gap flux density, simultaneously [16]. The complex permeance model assumes that the slot opening is infinitely deep, and it also cannot consider the interaction effect between adjacent slots. To resolve these problems, the SC Toolbox was used in [17-18]. In [17-18], the SC mapping was solved numerically by using the SC Toolbox. In real, the CM method presented in [17-18] is a semi-analytical method. In this paper, this semi-analytical method is used for investigating the influence of PM magnetization, PM shaping, and the slot opening shift on the performance of two typical PMSMs with integral and fractional slot

Submitted On: August 6, 2016
Accepted On: August 12, 2017

winding.

This paper is organized as follows: Section II introduces the CM method. The calculation of air gap magnetic field, and back-EMF are presented in Sections III-IV, respectively. Section V shows the cogging torque calculation and reduction for different configurations of PMs, and by using the slot opening shift method. Section VI gives conclusions.

II. CM METHOD

The CM method is an analytical and numerical tool for analysis of different 2-D fields, such as electrostatic, magnetostatic, and so on. The main parameters of two typical PMSM analyzed in this paper are presented in Table 1. In this paper, three CMs, including two logarithmic complex functions and the SC mapping, are used to reach the canonical domain.

Table 1: Main parameters of analyzed PMSMs

Parameter	Value and Unit
Number of pole pairs, p	2
Number of slots, Q_s	12 / 6
Winding type	Single layer / Double layer
Magnet remanence, B_r	0.96 T
Relative recoil permeability, μ_r	1.07
Rated frequency, f	50 Hz
Motor topology	Internal rotor
Magnetization	Radial
Stator outer diameter	130 mm
Stator inner diameter	75 mm
Active length, L	65 mm
Air gap length, g	1 mm
Magnet thickness	3.5 mm
Pole arc to pole pitch ratio, α_p	0.9 (radial and parallel magnetization) 1 (segmented Halbach magnetization, and sin-shaping)
Winding turns per coil, N_c	200
Rated voltage (V_{RMS})	170 (volts)

A. First logarithmic CM

The first CM is a logarithmic complex function as:

$$z = log(s). \quad (1)$$

The motor geometry in s-plane (physical domain) is transformed to z-plane using (1), as shown in Figs. 1 (a-b) for one typical PMSM with 6 slots and 4 poles.

B. Schwartz-Christoffel (SC) mapping

SC mapping is defined as follows:

$$z = f(w) = A\int \prod_{k=1}^{n-1}(w - w_k)^{-\frac{\alpha_k}{\pi}-1}\, dw + C, \quad (2)$$

where A and C are the integration constants, n is the number of polygon corners in z-plane, $w_k's$ are the points on the boundary in w-plane corresponding to the polygon corners, $\alpha_k's$ are the interior angles in polygon corners.

SC transformation $z = f(w)$ maps the canonical domain in w-plane to the interior or exterior of respective polygon in z-plane. The canonical domain in w-plane may be a rectangle, disk, bi-infinite strip, and upper or lower half-plane. In this paper, the canonical domain in w-plane is one rectangle.

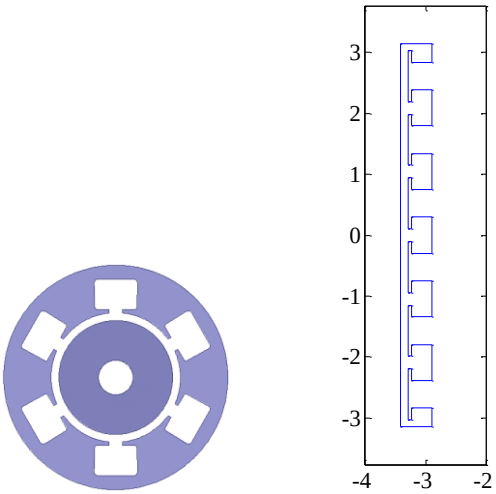

(a) s-plane (b) z-plane

Fig. 1. The motor geometry (6 slots/4 poles).

C. Second logarithmic CM

The third CM is also a logarithmic complex function, as follows:

$$w = j\left(log(\psi)\frac{\Delta x}{2\pi} + \frac{\Delta y}{2} - j\frac{\Delta x}{2}\right),$$
$$\Delta x = w(2) - w(1)\,,\ \Delta y = w(3) - w(2). \quad (3)$$

The canonical rectangle in w-plane is mapped to an annulus in ψ-plane by using (3). Figure 2 shows the main canonical domain in ψ-plane.

The selection of annulus as the main canonical domain has two main advantages. First, the boundary condition is applied automatically in ψ-plane. Second, the hague solution is known for an annular domain.

D. Hague's solution

Figure 2 shows an annulus including a line current located at $\psi = ce^{j\theta_1}$. The radii of stator and rotor in the main canonical domain (annular domain) are "a" and "b", respectively. The magnetic permeability of the stator core, air gap, and the rotor core are also μ_1, μ_2, and μ_3, respectively. Hague presents a solution for scalar magnetic potential in this annular domain as a function of r and θ, as [19]:

$$\Omega_\psi = \begin{cases} \frac{\mathrm{I}}{2} + \sum_{n=1}^{\infty}\left(\left(A_n - \frac{I}{2n\pi c^n}\right)r^n + B_n r^{-n}\right)\sin\left(n(\Delta\theta)\right), r < c \\ \frac{I(\Delta\theta+\pi)}{4\pi} + \sum_{n=1}^{\infty}\left(A_n r^n + B_n r^{-n}\right)\sin\left(n(\Delta\theta)\right), r = c \\ \frac{I\Delta\theta}{2\pi} + \sum_{n=1}^{\infty}\left(A_n r^n + \left(\frac{Ic^n}{2n\pi} + B_n\right)r^{-n}\right)\sin\left(n(\Delta\theta)\right), r > c \end{cases} \quad (4)$$

where

$$\begin{cases} A_n = \frac{-I(\mu_1-\mu_2)\{b^{2n}(\mu_3-\mu_2)+c^{2n}(\mu_3+\mu_2)\}}{c^n 2n\pi\left(b^{2n}(\mu_1-\mu_2)(\mu_2-\mu_3)+a^{2n}(\mu_1+\mu_2)(\mu_2+\mu_3)\right)}, \\ B_n = \frac{b^{2n}I(\mu_3-\mu_2)\{c^{2n}(\mu_1-\mu_2)+a^{2n}(\mu_1+\mu_2)\}}{c^n 2n\pi\left(b^{2n}(\mu_1-\mu_2)(\mu_2-\mu_3)+a^{2n}(\mu_1+\mu_2)(\mu_2+\mu_3)\right)}. \\ \Delta\theta = \theta - \theta_I \end{cases}$$

The air gap flux density in the main canonical domain is then calculated as:

$$B_\psi = -\mu_0 \nabla\Omega_\psi = -\mu_0\left[\frac{\partial\Omega_\psi}{\partial r}\overrightarrow{a_r} + \frac{1}{r}\frac{\partial\Omega_\psi}{\partial\theta}\overrightarrow{a_\theta}\right]. \quad (5)$$

The air gap flux density is similarly calculated for all line currents due to the armature winding and PMs.

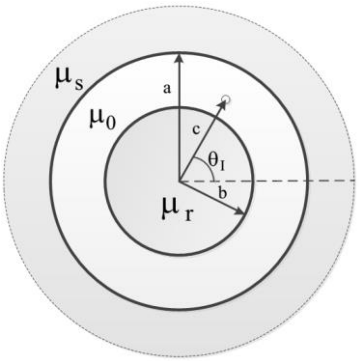

Fig. 2. The main canonical domain in ψ-plane.

E. Air gap complex permeance

The air gap flux density in the physical domain (s-plane) is calculated as [17]:

$$B_s = B_\psi\left(\frac{\partial\psi}{\partial s}\right)^* = \frac{B_\psi}{\left(\frac{\partial s}{\partial\psi}\right)^*} = B_\psi\left(\frac{1}{\frac{\partial w}{\partial\psi}}\right)^*\left(\frac{1}{\frac{\partial z}{\partial w}}\right)^*\left(\frac{\partial z}{\partial s}\right)^*, \quad (6)$$

$$B_s = B_r + jB_t$$

where

$$\frac{\partial w}{\partial\psi} = j\frac{\Delta x}{2\pi\psi}, \quad (7)$$

$$\frac{\partial z}{\partial w} = evaldiff(f, w), \quad (8)$$

$$\frac{\partial z}{\partial s} = \frac{1}{s}. \quad (9)$$

The complex permeance for the slotted air gap is defined as:

$$\lambda = \left(\frac{1}{\frac{\partial w}{\partial\psi}}\right)\left(\frac{1}{\frac{\partial z}{\partial w}}\right)\left(\frac{\partial z}{\partial s}\right), \quad (10)$$

$$\lambda = \lambda_r + j\lambda_t, \quad (11)$$

where λ_r and λ_t are respectively the radial and tangential components of slotted air gap complex permeance, and evaldiff (f, w) calculates the derivative of function "f" with respect to "w".

Figure 3 shows the radial and tangential components of air gap complex permeance for one typical PMSM with 6 slots and 4 poles. This figure shows the slotting effect with the period of one slot pitch.

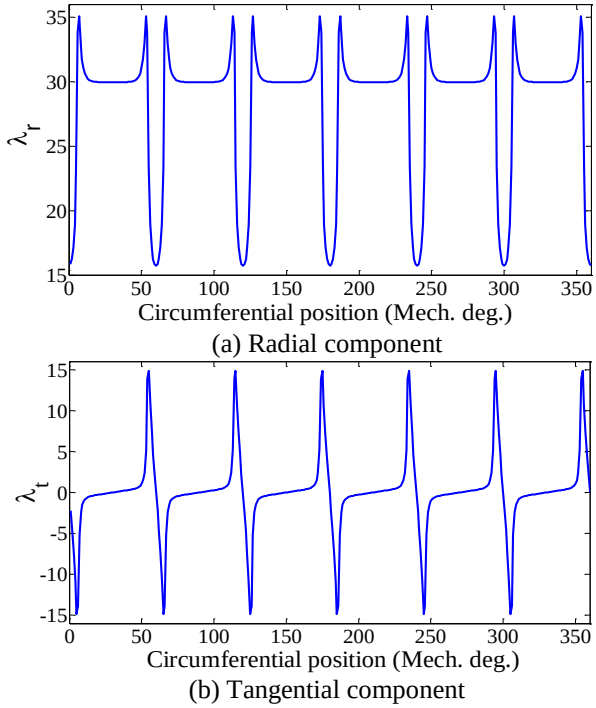

(a) Radial component

(b) Tangential component

Fig. 3. The components of air gap complex permeance.

F. Excitation modeling

All excitation, including PM and armature winding, are modeled by using equivalent line currents. For modeling the armature reaction, each coil side is easily replaced by using at least one equivalent line current. However, the PM equivalent line currents have to be calculated while considering the magnetization type.

The magnetization characteristic for each PM is usually written as:

$$\vec{M} = \frac{B_R}{\mu_0} + \left(\mu_r - 1\right)\vec{H} = M_r\overrightarrow{a_r} + M_t\overrightarrow{a_t}, \quad (12)$$

where B_R is the magnet remanence, μ_0 is the magnetic permeability of air, μ_r is the relative permeability of PM, and H is the magnetic field intensity inside PM due to the armature reaction.

The PM equivalent line currents are divided into two groups: the equivalent surface and volume currents. The densities of these PM equivalent currents are defined as:

$$J_s = \vec{M} \times \overrightarrow{a_n}\ \left(A/m\right), \quad (13)$$

$$J_v = \vec{\nabla} \times \vec{M}\left(A/m^2\right), \quad (14)$$

where $\overrightarrow{a_n}$ is the unit vector perpendicular to the PM surface.

Since the relative permeability of PMs is very close to one, therefore the PM magnetization distribution can assumed to be a uniform distribution. Consequently, the equivalent volume currents can be ignored in PM modeling.

For one PM with radial magnetization and radial sides, the equivalent surface currents exist only on lateral sides (Fig. 4). The magnitude of these equivalent surface currents are calculated as:

$$I_s = \frac{B_R}{\mu_0} \times \frac{l_m}{n_1}, \tag{15}$$

$$M = \frac{B_R}{\mu_0}, \tag{16}$$

where l_m is the magnet thickness, and n_1 is the number of equivalent currents on each lateral side of PMs.

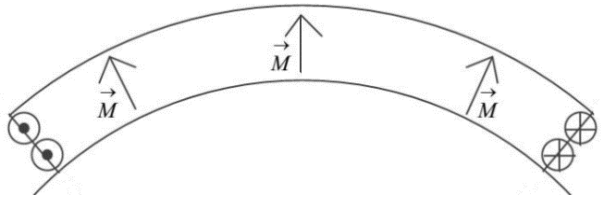

Fig. 4. The PM equivalent currents for radial magnetization.

For one PM with parallel magnetization, the equivalent surface currents also exist on the inner and outer arcs (Fig. 5). These equivalent surface currents are defined as:

$$J_s = \begin{cases} M \times \cos\left(\frac{\alpha_p \pi}{2p}\right) & \theta = \frac{\alpha_p \pi}{2p} \\ -M \times \cos\left(\frac{\alpha_p \pi}{2p}\right) & \theta = -\frac{\alpha_p \pi}{2p} \\ M \times \sin\theta & -\frac{\alpha_p \pi}{2p} \le \theta \le \frac{\alpha_p \pi}{2p}\ ,\ r = R_m \\ -M \times \sin\theta & -\frac{\alpha_p \pi}{2p} \le \theta \le \frac{\alpha_p \pi}{2p}\ ,\ r = R_r \end{cases} \tag{17}$$

$$I_s = J_s \times r \times d\theta,$$

where α_p is the pole arc coefficient, p is the number of pole pair, R_r is the inner radius of PM, R_m is the outer radius of PM, θ is the angular position of each surface element relative to the symmetrical axis of PM, and $d\theta$ is the arc length of each surface element in radian.

For one PM with segmented Halbach magnetization (Fig. 6), the equivalent surface currents exist on all sides of all PM segments. The radial and tangential components of magnetization vector $(\vec{M})$ for each PM segment are calculated as:

$$\begin{aligned} M_r &= M \times \sin\left(\alpha_i + (\theta - \theta_i)\right), \\ M_\theta &= M \times \cos\left(\alpha_i + (\theta - \theta_i)\right), \end{aligned} \tag{18}$$

where θ is the circumferential position on the surface of PM.

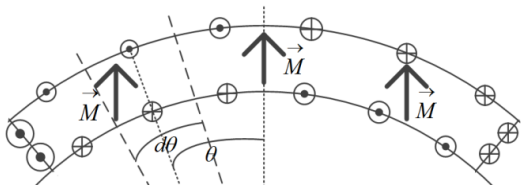

Fig. 5. The PM equivalent currents for parallel magnetization.

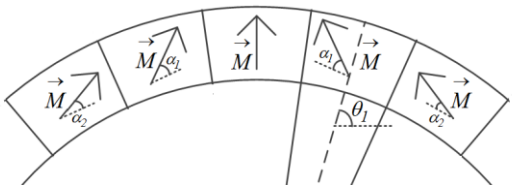

Fig. 6. PM with segmented Halbach magnetization.

For each PM segment with Halbach magnetization, the equivalent surface currents can be calculated while having the radial and tangential components of magnetization vector.

III. MAGNETIC FIELD CALCULATION

The radial and tangential components of air gap magnetic field are calculated by using (6). For radial and parallel magnetization, Fig. 7 shows the components of air gap magnetic field due to PMs (for PMSM with 12 slot/4 pole). As shown, the air gap field obtained through the parallel magnetized PMs is more sinusoidal than it obtained from the radial magnetized PM. However, it is still far from a suitable sinusoidal air gap field.

For creating a more sinusoidal air gap field, the Hat-type configuration and the sin-shaping are considered for PM poles with full pitch. As shown in Fig. 8, the segmented-Halbach magnetization is selected for each PM pole in Hat-type configuration. Figure 9 also shows one typical PM pole with sin-shaping and parallel magnetization. In Fig. 9, ξ shows the eccentricity value of outer arc of PM pole relative to the rotor center, R_m is radius of outer arc, h_{min} and h_{max} are respectively the minimum and maximum thickness of PM poles. To reduce the harmonic content of air gap magnetic field, the optimal configurations of Hat-type and sin-shaped magnet poles are obtained as shown in Tables 2-3.

Table 2: Optimal parameters of Hat-type poles

Optimal Widths	Optimal Orientations	Optimal Thickness
$w_1 = 40^\circ$	$\alpha_1 = 90^\circ$	$l_1 = 3.5\ (mm)$
$w_2 = 15^\circ$	$\alpha_2 = 75^\circ$	$l_2 = 2.6\ (mm)$
$w_3 = 10^\circ$	$\alpha_3 = 37.5^\circ$	$l_3 = 1.56\ (mm)$

Table 3: Optimal parameter of sin-shaped poles

ξ	R_m	h_{min}	h_{max}
8.2 (mm)	28.3 (mm)	0.5 (mm)	3.5 (mm)

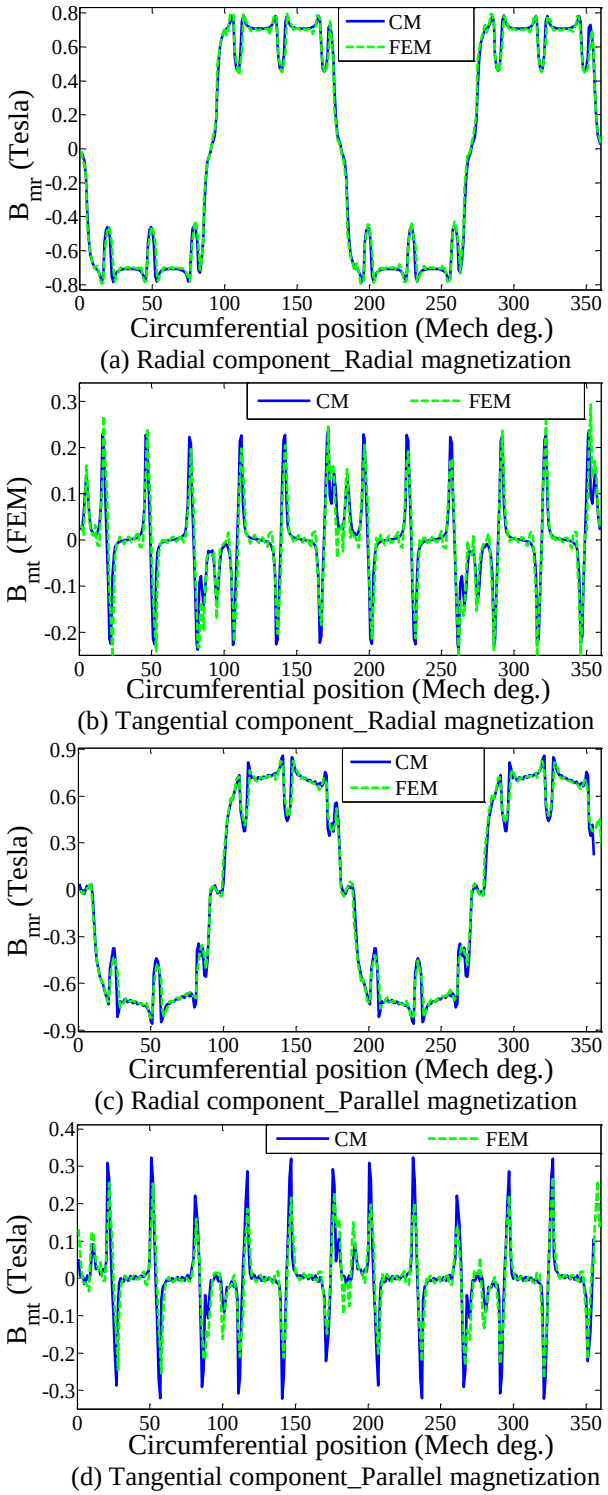

Fig. 7. The components of air gap magnetic field.

For these optimal configurations, Fig. 10 shows the radial components of air gap magnetic field due to PMs (for PMSM with 12 slot/4 pole).

Table 4 compares the total harmonic distortion (THD) of B_{mr} obtained through the analyzed PMSM (12 slot/ 4 pole) while considering the radial magnetization, parallel magnetization, optimal Hat-type configuration, and optimal sin-shaped pole. As shown, the air gap magnetic field obtained through sin-shaped configuration is more sinusoidal than others.

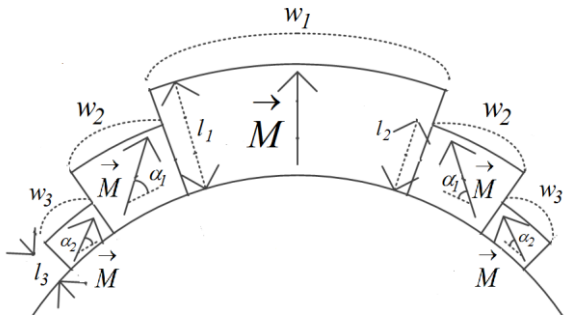

Fig. 8. Hat-type configuration with segmented Halbach magnetization.

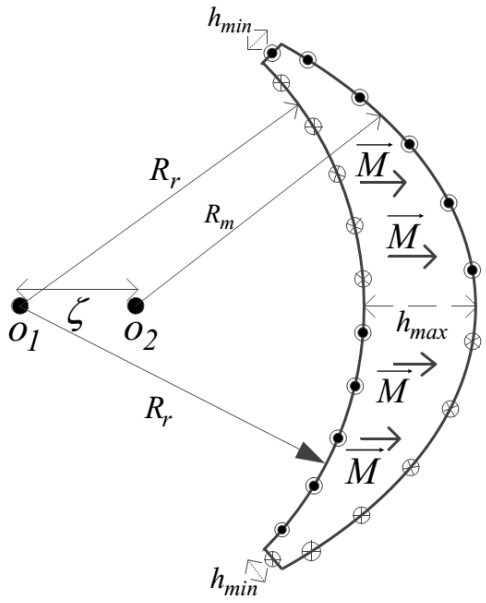

Fig. 9. Sin-shaped PM pole with parallel magnetization.

Table 4: THD comparison of B_{mr}

	Radial Magnetization	Parallel Magnetization	Optimal Hat-type	Optimal Sin-shape
THD	40.5%	27.37%	15.6%	10.8%

IV. BACK-EMF CALCULATION

The PM flux-linkage and back-EMF can be calculated

for each phase while having the distribution of air gap magnetic field and phase windings

$$\lambda_m = R_g.L\int_0^{2\pi} n_A(\varphi).B_{mr}(\varphi)\,d\varphi, \quad (19)$$

$$E_m = \frac{d\lambda_m}{dt}, \quad (20)$$

where R_g is the radius of integration contour in the middle of air gap, L is the axial length of the core, n_A is the turn function of phase A, B_{mr} is the radial component of air gap field, λ_m is the PM flux-linkage of phase A, and E_m is the PM back-emf of phase A.

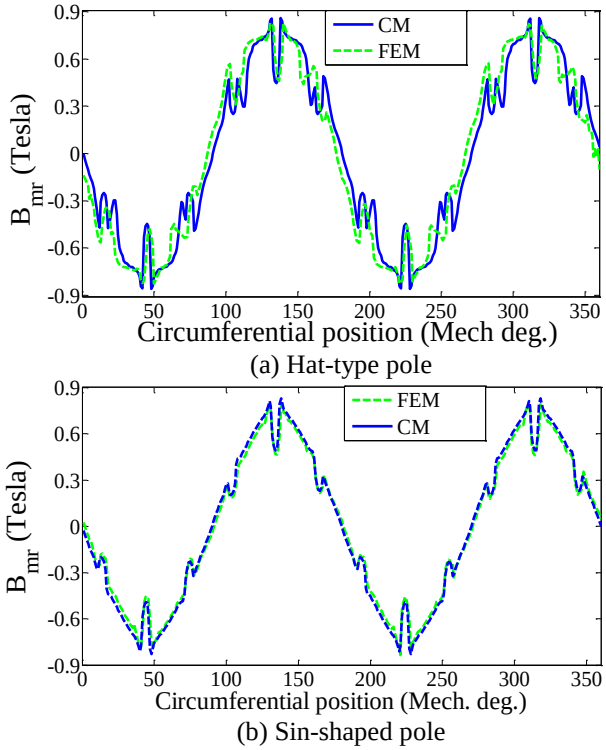

Fig. 10. Radial components of air gap field obtained through optimal Hat-type and sin-shaped configurations.

Figure 11 shows the PM back-EMF for an analyzed PMSM with 12 slots and 4 poles while considering different magnetizations and shaping for PMs. As shown, the back-EMF waveform is more sinusoidal for sin-shaped PM poles than others.

Figure 12 shows the optimal PM back-EMF obtained through two analyzed PMSMs (12s/4p, and 6s/4p). Table 5 compares these optimal results in terms of THD. As shown, the optimal PM back-EMF obtained through PMSM 6s/4p is more sinusoidal than the other.

Table 5: THD comparison of optimal back-EMFs

	12 slot / 4 pole	6 slot / 4 pole
THD	5.2%	1.8%

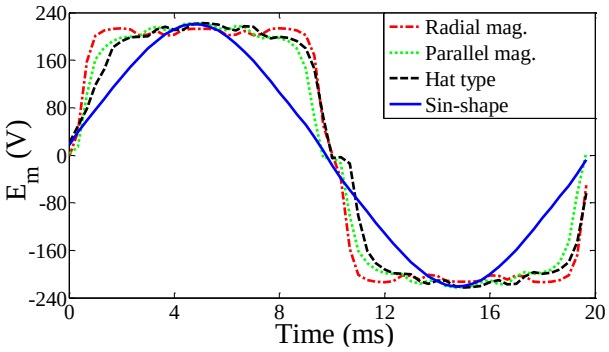

Fig. 11. Back-EMF comparison.

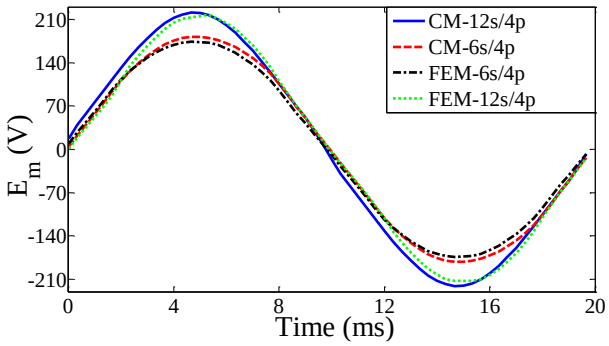

Fig. 12. Optimal PM back-EMFs.

V. COGGING TORQUE

A. Cogging torque calculation

One of the main drawbacks of PM machines, particularly in integral slot PM motor, is the cogging torque. Cogging torque is the main cause of torque pulsation and results in the shaft vibration and acoustic noise. In real, cogging torque is due to the interaction effect between the rotor PMs and the stator teeth. In this paper, Maxwell Stress Tensor (MST) method is used to calculate the cogging torque as follows:

$$T_c = \frac{L.R_g^2}{\mu_0}\int_0^{2\pi} B_{mr}.B_{mt}\,d\theta, \quad (21)$$

where B_{mt} is the tangential component of air gap field due to PMs.

Figure 13 shows the cogging torque waveforms for different configurations of analyzed PMSMs. For clarity in comparison, the cogging torque waveforms are shown in Fig. 13 (a) except for sin-shaped configuration. The comparison between Figs. 13 (a & b) shows the extreme influence of sin-shaped PM poles on the cogging torque reduction. In real, by using the sin-shaped PM poles, the peak to peak value of cogging torque waveforms for PMSMs 12s/4p and 6s/4p are respectively reduced about 95% and 97% in comparison to the configuration with radial magnetized PMs. Figure 13 (b) also shows that the PMSM 6s/4p is more effective than the PMSM 12s/4p

for cogging torque reduction, so that the ratio of peak to peak value of T_c $(T_{c,p-p})$ for analyzed PMSMs is as follows:

$$\frac{T_{c,p-p,6s/4p}}{T_{c,p-p,12s/4p}} \cong 0.36.$$

B. Slot opening shift method

The design technique for cogging torque reduction can be divided into two general groups, as follows:

- ✓ Rotor design techniques;
- ✓ Stator design techniques.

The magnet shaping technique is in the first category. In this paper, the technique of slot opening shift is also implemented on the stator simultaneous with using of sin-shaped PMs on the rotor. The technique of slot opening shift is in the second category, and it has no side effect on the motor performance such as the air gap field, back-EMF, and average torque.

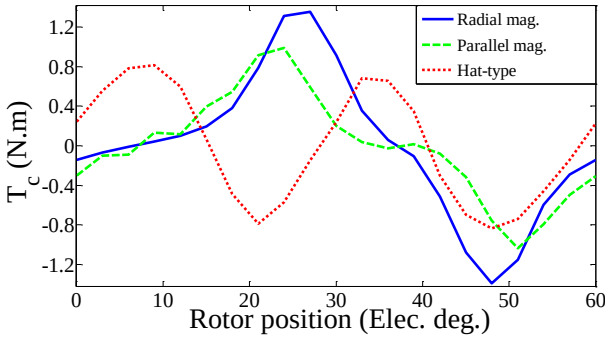

(a) PMSM 12s/4p

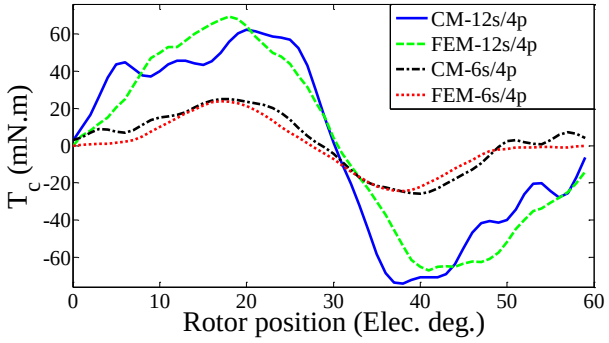

(b) Sin-shaping of PMs

Fig. 13. Cogging torque comparison.

In the slot opening shift method, the γ adjacent slots take as a group. It is obvious that γ should be equal to the number of cogging torque periods per pole, as follows:

$$\gamma = \frac{N_c}{2p}, \tag{22}$$

where N_c equals to the least common multiple of the number of stator slots N_s and the rotor poles $2p$. γ equals to 3 slots for both analyzed PMSMs. Therefore, all stator slots are divided into 4 groups for PMSM 12s/4p and 2 groups for PMSM 6s/4p. The optimization variables (angular shift of the slot opening position for each slot group) are defined.

For PMSM 12s/4p:

$$\begin{cases} -5^\circ \le \theta_1 \le 0^\circ \\ 0^\circ \le \theta_2 \le 5^\circ \end{cases} \rightarrow \begin{cases} \theta_{1,optimal} = -4.25^\circ \\ \theta_{2,optimal} = 5^\circ \end{cases}.$$

For PMSM 6s/4p:

$$\begin{cases} -11^\circ \le \theta_1 \le 0^\circ \\ 0^\circ \le \theta_2 \le 11^\circ \end{cases} \rightarrow \begin{cases} \theta_{1,optimal} = -4^\circ \\ \theta_{2,optimal} = 10.5^\circ \end{cases}.$$

These optimal results are obtained by using the genetic algorithm. Figure 14 shows the final optimal model for PMSMs 12s/4p and 6s/4p while considering the shifted slot openings on the stator and the sin-shaped PMs on the rotor, simultaneously.

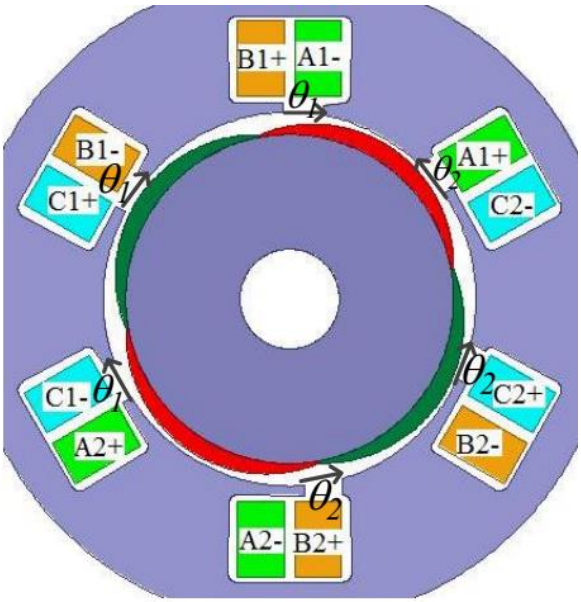

(a) PMSM 6s/4p

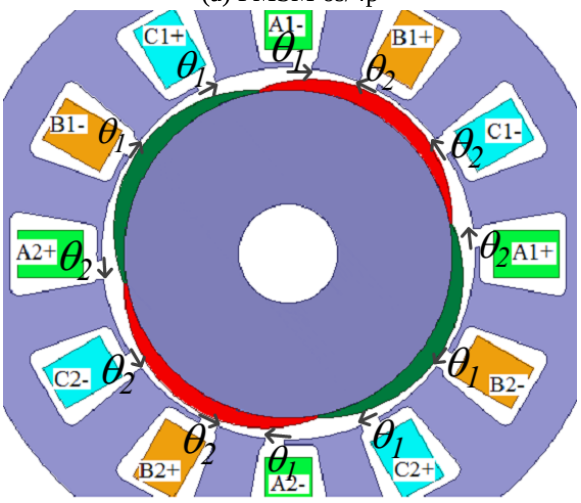

(b) PMSM 12s/4p

Fig. 14. Final optimal models.

Figures 15-16 show the waveforms of cogging torque and PM back-EMF obtained through optimal PMSMs. As seen from Fig. 15, the peak to peak value of cogging torque is extremely reduced (about 98.8%) in comparison to the PMSMs with radial magnetized PMs.

Figure 16 also shows that the technique of slot opening shift has no side effect on the sinusoidal back-EMF obtained through PMSMs with sin-shaped PMs.

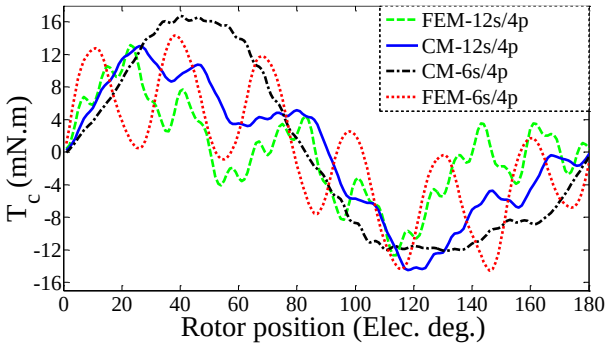

Fig. 15. Optimal waveforms of cogging torque.

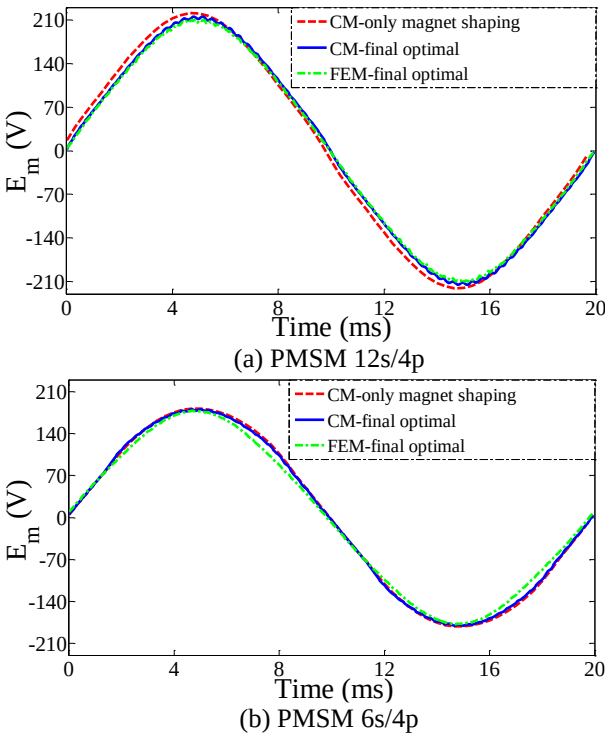

Fig. 16. Optimal waveforms of PM back-EMF.

VI. CONCLUSION

In this paper, by using the CM method as an accurate and fast method, a new optimal design was presented for PMSMs (either integral or fractional slot), which can include different design considerations. This new optimal configuration included the sin-shaped magnet poles on the rotor with shifted slot openings on the stator. The air gap magnetic field is sinusoidal by using this technique of magnet shaping. This hybrid technique simultaneously leads to an ideal PM back-EMF and the extreme reduction in the cogging torque without any destructive effect on the motor performance. This important feature distinguishes this new optimal design from other techniques which have been presented so far. Without using the technique of slot opening shift, the results show that the fractional slot PMSMs are more optimal than the integral slot PMSMs. However, by using the shifted slot opening on the stator in simultaneous with the magnet shaping technique, the obtained results are fairly similar for both fractional and integral slot PMSMs. The using of slot opening shift method has no side effect on the motor performance.

REFERENCES

[1] J. Wang and D. Howe, "Tubular modular permanent-magnet machines equipped with quasi-Halbach magnetized magnets--Part I: Magnetic field distribution, EMF, and thrust force," *IEEE Trans. Magn.*, vol. 39, no. 3, pp. 1793-1799, 2003.

[2] P. Zheng, J. Zhao, J. Han, J. Wang, Z. Yao, and R. Liu, "Optimization of the magnetic pole shape of a permanent-magnet synchronous motor," *IEEE Trans. Magn.*, vol. 43, no. 6, pp. 2531-2533, 2007.

[3] K. Wang, Z. Q. Zhu, and G. Ombach, "Torque improvement of five-phase surface-mounted permanent magnet machine using third-order harmonic," *IEEE Trans. Energy Convers.*, vol. 29, no. 3, pp. 735-747, 2014.

[4] Y. Li, J. Xing, T. Wang, and Y. Lu, "Programmable design of magnet shape for permanent-magnet synchronous motors with sinusoidal back EMF waveforms," *IEEE Trans. Magn.*, vol. 44, no. 9, pp. 2163-2167, 2009.

[5] Y. Shen and Z. Q. Zhu, "Investigation of permanent magnet brushless machines having unequal-magnet height pole," *IEEE Trans. Magn.*, vol. 48, no. 12, pp. 4815-4830, 2012.

[6] S. M. Jang, H. Park, J. Y. Choi, K. J. Ko, and S. H. Lee, "Magnet pole shape design of permanent magnet machine for minimization of torque ripple based on electromagnetic field theory," *IEEE Trans. Magn.*, vol. 47, no. 10, pp. 3586-3589, 2011.

[7] W. Fei and Z. Q. Zhu, "Comparison of cogging torque reduction in permanent magnet brushless machines by conventional and herringbone skewing techniques," *IEEE Trans. Energy Convers.*, vol. 28, no. 3, pp. 664-674, 2013.

[8] C. Xia, Z. Zhang, and Q. Geng, "Analytical modeling and analysis of surface mounted permanent magnet machines with skewed slots," *IEEE Trans. Magn.*, vol. 51, no. 5, Article#: 8104508, 2015.

[9] K. Abbaszadeh, F. Rezaee Alam, and S. A. Saied, "Cogging torque optimization in surface-mounted permanent-magnet motors by using design of experiment," *Energy Convers. Manage*., vol. 52, no. 10, pp. 3075-3082, 2011.

[10] Z. Q. Zhu and D. Howe, "Influence of design parameters on cogging torque in permanent magnet motors," *IEEE Trans. Energy Convers.*, vol. 15, no. 4, pp. 407-412, 2000.

[11] M. Gulec and M. Aydin, "Magnet asymmetry in reduction of cogging torque for integer slot axial flux permanent magnet motors." *IET Electr. Power Appl*., vol. 8, no. 5, pp. 189-198, 2014.

[12] C. Liu, J. Zhu, Y. Wang, G. Lei, and Y. Guo, "Cogging torque minimization of SMC PM transverse flux machines using shifted and unequal-width stator teeth," *IEEE Trans. Appl. Supercond.*, vol. 26, no. 4, Article#: 5204704, 2016.

[13] Z. Q. Zhu, L. J. Wu, and Z. P. Xia, "An accurate subdomain model for magnetic field computation in slotted surface-mounted permanent-magnet machines," *IEEE Trans. Magn.*, vol. 46, no. 4, pp. 1100-1115, 2010.

[14] Z. J. Liu and J. T. Li, "Accurate prediction of magnetic field and magnetic forces in permanent magnet motors using an analytical solution." *IEEE Trans. Energy Conversion*, vol. 23, no. 3, pp. 717-726, Sep. 2008.

[15] Z. Q. Zhu and D. Howe, "Instantaneous magnetic field distribution in brushless permanent magnet dc motors. Part III: Effect of stator slotting," *IEEE Trans. Magn.*, vol. 29, no. 1, pp. 143-151, 1993.

[16] D. Zarko, D. Ban, and T. A. Lipo, "Analytical calculation of magnetic field distribution in the slotted air gap of a surface permanent-magnet motor using complex relative air-gap permeance," *IEEE Trans. Magn.*, vol. 42, no. 7, pp. 1828-1837, 2006.

[17] T. C. O'Connell and P. T. Krein, "A Schwarz-Christoffel-based analytical method for electric machine field analysis," *IEEE Trans. Energy Convers*., vol. 24, no. 3, pp. 565-577, 2009.

[18] F. Rezaee Alam and K. Abbaszadeh, "Magnetic field analysis in eccentric surface-mounted permanent-magnet motors using an improved conformal mapping method," *IEEE Trans. Energy Convers*., vol. 31, no. 1, pp. 333-344, Nov. 2015.

[19] B. Hague, *Electromagnetic Problems in Electrical Engineering*. London, U.K.: Oxford Univ. Press, 1929.